Deposition, diffusion and aggregation of atoms on surfaces: A model for nanostructure growth

Pablo Jensen,* Albert-László Barabási,† Hernán L.arralde,‡ Shlomo Havlin,§ and H. E. Stanley
Center for Polymer Studies and Department of Physics, Boston University, Boston, Massachusetts 02215
(Received 5 July 1994)

We propose a model that describes the diffusion-controlled aggregation exhibited by particles as they are deposited on a surface. The model, which incorporates deposition, particle and cluster diffusion, and aggregation, is inspired by recent thin-film-deposition experiments. We find that as randomly deposited particles diffuse and aggregate they configure themselves into a wide variety of fractal structures characterized by a length scale L_1. We introduce an exponent γ that tunes the way the diffusion coefficient changes with cluster size: if the values of γ are very large, only single particles can move, if they are smaller, all clusters can move. The introduction of cluster diffusion dramatically affects the dynamics of film growth. We compare our results with those of several recent experiments on two-dimensional nanostructures formed by diffusion-controlled aggregation on surfaces, and we propose several experimental tests of the model. We also investigate the spanning properties of this model and find another characteristic length scale L_2 ($L_2 \gg L_1$) above which the system behaves as a bond percolation network of the fractal structures each of length scale L_1. Below L_2, the system shows similarities with diffusion-limited aggregation. We find that L_1 scales as the ratio of the diffusion constant over the particle flux to the power 1/4, whereas L_2 scales with another exponent close to 0.9.

I. INTRODUCTION

Understanding the processes underlying the growth of thin films has led to widespread interest, both from physical and technological points of view.[1–9] *Equilibrium* (thermodynamic) models have been developed and applied with some success to the film-substrate system.[1,2] However, improvements in experimental techniques—such as scanning tunneling microscopy—permit the investigation of atomic details of the embryonic submonolayer stages of nanostructure film growth, and recent experimental works[10,11] have recognized the importance of *out-of-equilibrium* (kinetic) effects on the formation of the observed morphologies.

Addressing such out-of-equilibrium effects is important if one is to be able to control the morphology of submonolayer nanostructures. One might consider the use of the percolation model to describe certain experiments of surface deposition.[12] However, percolation assumes that particles do not diffuse after being deposited, when in fact not only diffusion but also aggregation of the diffusing particles takes place. There exist models of diffusing particles that aggregate, but such "cluster-cluster aggregation" (CCA) models[13] do not allow the continual injection of new particles via deposition. Here we develop a model that incorporates the three physical ingredients of thin-film growth: deposition, diffusion, and aggregation (DDA). Similar models that neglect the shape of the islands or the possibility of cluster diffusion were studied independently.[3,4] We introduce the possibility of *cluster* diffusion and we also investigate the *spanning* properties of the system. These two topics have been neglected in previous studies of similar models.[3,4] The importance of these novelties, from both the experimental and theoretical points of view, will be explained in the subsequent sections.

We show in the following that the DDA model generates a wide variety of fractal structures characteristic of different models such as percolation,[14,15] diffusion limited aggregation (DLA),[16,17] or CCA. The introduction of *cluster* diffusion moves this model away from the universality class of previous models with the introduction of new scaling exponents. Moreover, it leads to an *exponential* increase in the mean cluster size as a function of time, whereas in other growth models[3,4,17] this dependence is a power law.

II. MODEL DESCRIPTION AND JUSTIFICATION

The DDA model is defined as follows (Fig. 1).

(1) *Deposition.* Particles are deposited at randomly chosen positions of the surface at a flux F per lattice site per unit time.

(2) *Diffusion.* All particles and clusters (sets of connected particles) are chosen at random and attempted to move north, east, south, or west by one lattice constant per unit time. The probability that they actually move is proportional to their mobility, which we assume to be given by $D_s = D_1 s^{-\gamma}$. Here s is the number of particles in the cluster, D_1 is the diffusion coefficient for a monomer ($s = 1$), and the parameter γ characterizes the dependence of D_s on cluster size.

(3) *Aggregation.* If two particles come to occupy neighboring sites, they (and, therefore, the clusters to which

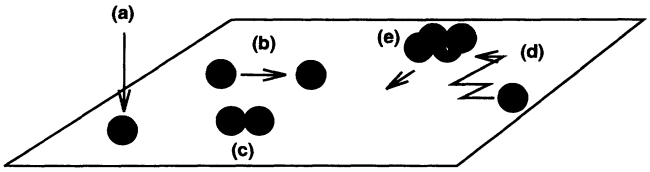

FIG. 1. Schematic representation of the basic processes considered in this model: (a) deposition, (b) and (d) particle diffusion, (e) island diffusion, and (c) aggregation. (b) corresponds to *nucleation* [i.e., a new island (c) is created] while (d) corresponds to *growth* of an already existing island (see the text for details).

they belong) stick irreversibly.

We call *particles* the isolated atoms (or monomers) that are deposited on the surface, *clusters* any set of connected particles (including the monomers), and *islands* the clusters containing more than one particle. Physically, two competing mechanisms are introduced in the model, each one with its own time scale: deposition and diffusion. It is useful to introduce the normalized flux defined as the number of particles deposited per unit site per *diffusion time* τ, where τ is the mean time needed by a monomer to jump by a lattice site. The monomer diffusion coefficient is then given by $D_1 = 1/(4\tau)$, and the normalized flux by $\phi = F\tau$. Then, from experimental values of F and D_1 it is possible to calculate ϕ and the morphologies predicted by our model. The program actually calculates a probability for dropping a particle: $p_{\rm drop} = \phi L^2/(\phi L^2 + N_{\rm cl})$ where L is the system size and $N_{\rm cl}$ is the total number of clusters present in the system. A random number p is chosen and compared to $p_{\rm drop}$. If $p < p_{\rm drop}$, a particle is added at a random position on the lattice. If $p > p_{\rm drop}$, a cluster or a particle is chosen at random and attempted to move. In both cases, the time is increased by $\tau/(\phi L^2 + N_{\rm cl})$.

Some remarks on the assumptions of this simple model regarding its connection to the experiments are now addressed.

(1) *Island diffusion.* Experimentally, two cases have to be distinguished concerning island diffusion. For epitaxial systems [as obtained in molecular beam epitaxy (MBE)], it has been argued that clusters larger than the dimer are practically immobile. This case can be modeled by taking a large value of γ (typically 10). For nonepitaxial systems, the situation is less clear. Experiments on metal deposition on ionic substrates have shown that the diffusion coefficient of clusters of size N varies as $D_N = D_0 N^{-2/3}, \exp(-E_a/k_B T)$ which gives $\gamma = 2/3$,[18] and that clusters containing several hundredths of particles can move on the substrate.[18–20] Moreover, studies of deposition of *compact*, preformed large molecules containing more than 1000 atoms have shown that these large molecules *do diffuse* on the surface at room temperature.[21,22] Therefore, in order to keep the DDA model as close as possible to experiments and as general as possible, we include a *tunable* parameter γ that characterizes the dependence of a cluster diffusivity on its size. Clearly, the experimental situations where cluster diffusivity is expected to be negligible can be modeled by choosing a large γ. Another point should be made about the diffusion mechanism of the large clusters in the DDA model. It seems clear that, even in systems where large clusters do diffuse, the diffusion is not *rigid*, in the sense that the cluster may change its internal structure to be able to move. Several tentative possibilities for these diffusion mechanisms are given in Ref. 1. This results typically in compact shapes for the clusters [see also remark (3) concerning edge diffusion]. In this sense, the rigid diffusion mechanism assumed in the model is not realistic for large clusters diffusing on surfaces. Rigid diffusion might be interesting in other contexts, such as colloids. However, for *small* clusters containing less than 10 sites, the clusters are rather compact and it can be speculated that the deformations needed to move do not significantly alter their shape: then the DDA model should reproduce well the effects of the diffusion of small clusters. From the theoretical point of view, it is interesting to find out whether the introduction of cluster diffusion introduces new universality classes as compared to previous models[3,4] which can be described by the "rate equations" (see Sec. III).

(2) *Second layer.* When a particle "falls" on top of another particle (i.e., is deposited in an already occupied site), we assume that the particle deposited on the second layer has no effect on the system. This means that the model is mainly suited for experimental systems where (i) there is a barrier at the edges of the (first layer) clusters which prevents single particles from falling on the substrate. The existence of such a "Schwoebel" barrier has been suggested in the study of terrace formation[23] and/or (ii) particle diffusion on the second layer is much smaller than diffusion on the substrate. This may happen because second-layer particles diffuse on a substrate formed by particles of the *same* element, while first-layer particles diffuse on the substrate, which is generally made up by another element.

(3) *Edge diffusion.* The diffusion of the adatoms that reach the already formed clusters is neglected in the present "zeroth-order" model, i.e., as specified in (c), particles stick *irreversibly* upon contact. Indeed, at low temperatures edge diffusion is probably not relevant, due to the higher activation energy for the edge diffusion in comparison to the "simple" surface diffusion. However, at higher temperatures, edge diffusion may influence the cluster morphology. We intend to take into account edge diffusion in future work on this model.

It should be stressed that this is only a zeroth-order model which has the ambition to give a feeling on the relative influence of deposition and diffusion on the growth properties of films. Details specific to certain experimental systems, such as the existence of the Schwoebel barrier, the precise dependence of cluster diffusion on size, etc., are not carefully taken into account since we want to keep the DDA model as general as possible. We could focus on detailed models specific to precise experimental systems: for example, we could include anisotropic diffusion[8,24] for Si-on-Si(001), but this is not our purpose here. We only wish to capture the essential physical ingredients involved in most deposition experiments (in

this case: deposition, diffusion, and aggregation) and try to understand the influence of each.

In the following section, we investigate briefly the way the particles deposited on the substrate aggregate, and the morphologies generated, in the case of large systems where finite-size effects are negligible. We compare our results to those obtained in previous models[3,4] where only monomers diffuse.

III. DYNAMICAL EVOLUTION

A. Simulation results

We give here a brief presentation of the growth properties of the model. Figure 2 shows snapshots of the system at four different coverages for a normalized flux 10^{-5}, a

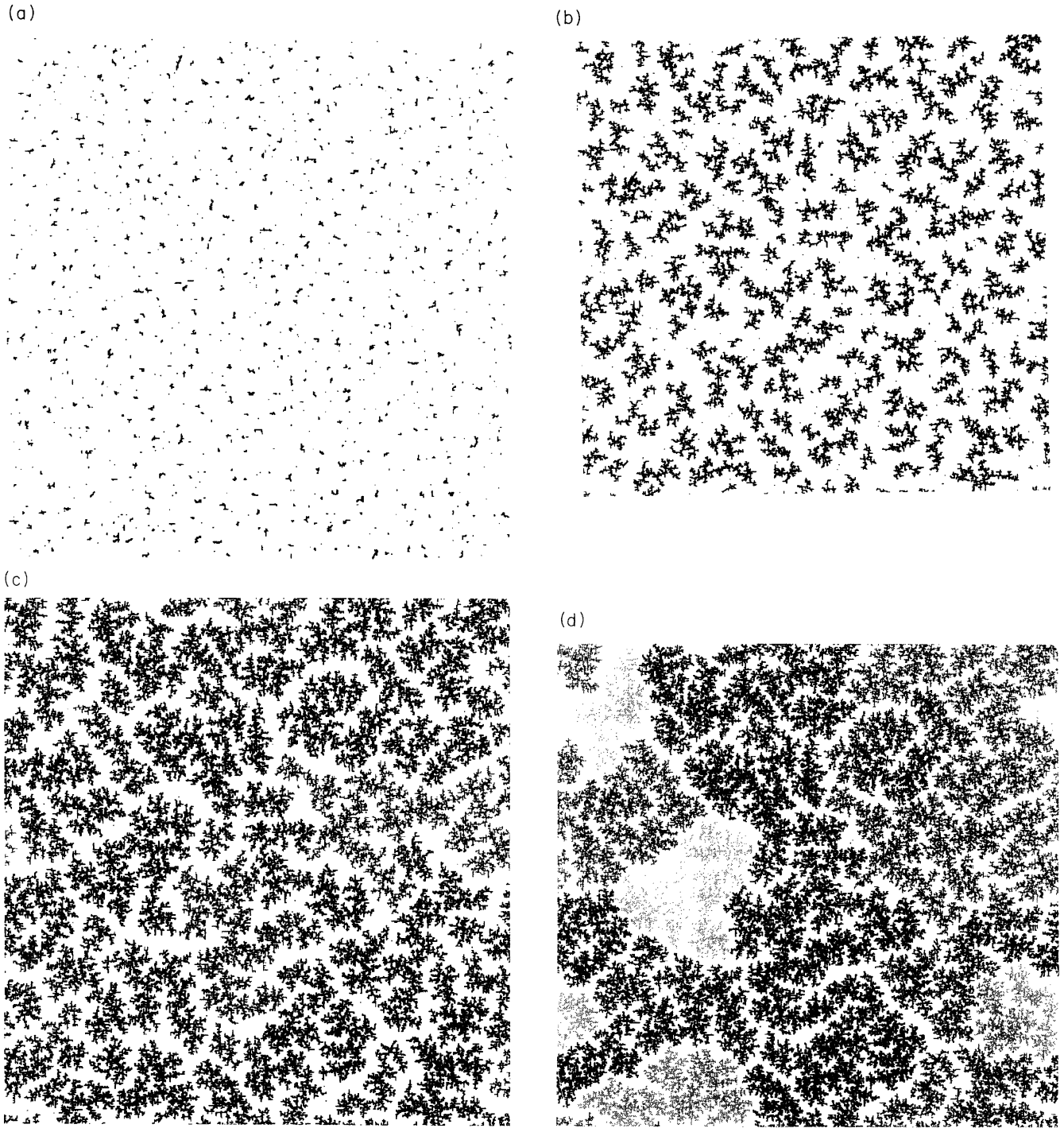

FIG. 2. Morphologies obtained for a normalized flux $\phi = 10^{-5}$, a system size $L = 500$ and $\gamma = 1$. Four different coverages (corresponding to four different times of deposition) are shown: (a) coverage 0.02, (b) coverage 0.15, (c) coverage 0.35, and (d) coverage 0.43 (spanning point).

system size $L = 500$ and $\gamma = 1$. The coverage is defined as the ratio of the number of occupied sites to the total number of sites on the surface. At very short times ($\theta \leq 0.001$), mainly monomers (isolated particles) are found on the substrate, since they did not yet meet another one to form a cluster [Fig. 3(a)]. Later, small clusters are homogeneously grown on the surface [Fig. 2(a)], and the island density (i.e., the number of islands per lattice site) starts to grow [Fig. 3(a)]. These small clusters can be considered, loosely speaking, as the "nucleation centers" for the growth.[25] As time increases, large clusters (henceforth called "blobs") grow on these nucleation centers, because of the diffusion of the clusters and also by addition of single particles [Fig. 2(b)]. It is interesting to characterize the morphology of the clusters by measuring their "effective" fractal dimension as a function of the coverage. This effective fractal dimension is obtained by plotting, for each cluster, its gyration radius versus its mass (number of sites): the effective fractal dimension is defined as the inverse slope of a linear fit to these points (see Ref. 17). From Fig. 2(a) to Fig. 2(b), the effective fractal dimension of the clusters increases from 1.45 to 1.65 [Fig. 3(b)]. This is so because at the beginning, the growth mechanism is very similar to the first stages of CCA, where clusters meet on a surface by pure diffusion. Thus the effective fractal dimension of the clusters is expected to be close to that measured in CCA (1.45–1.5, see, Ref. 17). As time increases however, larger clusters are grown whose diffusion is considerably reduced according to the $D_s = D_1 s^{-\gamma}$ law. Then, the main mechanism governing cluster growth is the addition of *single* particles. Thus the clusters tend to resemble DLA clusters, which are built only by addition of single particles. Therefore, their effective fractal dimension goes up to

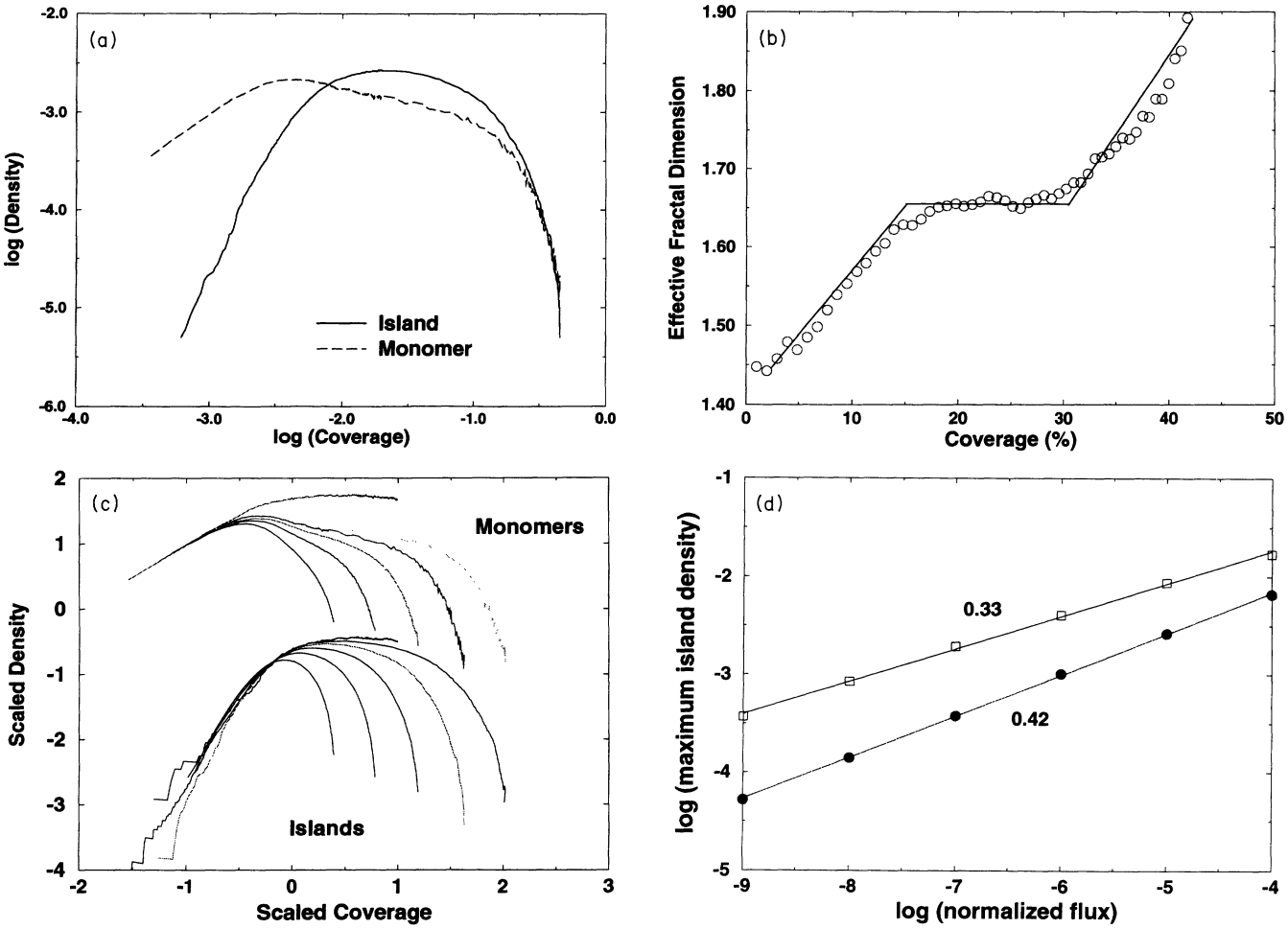

FIG. 3. (a) Densities of monomers and islands (clusters containing at least two particles) as a function of the coverage. These curves were obtained for a normalized flux $\phi = 10^{-5}$ and a system size $L = 1000$. (b) Fractal dimension of the clusters as a function of the total coverage for a normalized flux $\phi = 10^{-5}$, and a system size $L = 1000$. For each cluster, we plot its gyration radius versus its mass (number of sites): D_f is defined as the inverse slope of a linear fit to these points (see Ref. 17). The solid line indicates the crossover between the three "asymptotic" regimes. (c) Scaling of island and monomer densities according to Ref. 3 for $\phi = 10^{-7}$, 10^{-6}, 10^{-5}, 10^{-4}, 10^{-3}, *and* 10^{-2}. The scaled coverage is defined as $\theta/[\phi \log_{10}(2\theta/\phi)]^{1/2}$ and the scaled density as $N_{\rm isl}/[\phi \log_{10}(2\theta/\phi)]^{1/2}$. (d) Dependence of the maximum island density (number of islands divided by the total number of sites of the substrate) on the normalized flux. The circles represent the case $\gamma = 1$, while the squares show the densities obtained when only monomers diffuse.

1.65, very close to the fractal dimension of the DLA clusters. This (DLA-like) growth mechanism goes on until the linear dimension of the clusters becomes comparable to the separation between them, and the effective fractal dimension of the clusters stays close to 1.65. When the cluster radius becomes comparable to the separation between them [Fig. 2(c)], many particles start to fall *inside* the clusters and their effective fractal dimension rapidly increases [Fig. 3(b)]. Large clusters are built up by diffusion of the blobs and the blobs become denser by the addition of particles *inside* them. Eventually, a cluster of a size comparable to the system size is built and the system spans [Fig. 2(d)]. At that time, the effective fractal dimension of the spanning cluster reaches a value close to 1.9 [Fig. 3(b)]. The continuous increase of the effective fractal dimension seen in Fig. 3(b) can be explained by introducing three asymptotic regimes, each with a well-defined fractal dimension: CCA (1.45), DLA (1.7), and percolation (1.9). Asymptotically, for very low fluxes, one expects rapid jumps between these values of D_f as the coverage increases. For the flux investigated in Fig. 3(b), the finite size of the blobs results in a continuous variation of the effective fractal dimension. This analysis is supported by the fact that sharper jumps are observed for lower values of the normalized flux where the blobs are larger ($\phi = 10^{-6}$, not shown).

B. Discussion

We now attempt a brief analysis of the previous results in the framework of preceding studies.[1,3]

Scaling with the flux. Tang[3] has analyzed the growth mechanisms of his model in the framework of the "rate equations,"[1] a mean-field approach where islands are treated as *point* objects and only monomer diffusion is allowed. This analysis leads to scaling relations of the island and monomer density as a function of the coverage for different fluxes.[1,3] Particularities of random walks in two dimensions introduce logarithmic corrections.[3] The modified scaling relations[3] are in agreement with the numerical results only at small times, when the shape of the islands is unimportant. At small times, the islands are separated by a distance much larger than their radius; this explains that they can be treated as "point" objects. We also expect these scaling relations to apply to our simulations at early times, when the effects of island diffusion are negligible. Figure 3(c) shows that, indeed, the scaling relations are well verified by our numerical results too. However, we note that the range of agreement is smaller than the range found in Ref. 3. The analysis using the rate equations do not represent a satisfactory treatment for higher coverages, even for models without cluster diffusion, for many different reasons: the shape of the islands, the correlations in particle positions, the coalescence of the islands among others.

Maximum cluster density. A calculation for the *maximum* number of islands that takes into account their fractal dimension has been proposed.[3] We now show that this formula does not apply to the DDA model, certainly because of cluster diffusion. According to Ref. 3, the *maximum* island density $N_{\max}$ scales with the flux as

$$N_{\max} \sim \phi^{\zeta}, \tag{1}$$

where

$$\zeta = 2/(4 + d_f) \tag{2}$$

and d_f is the fractal dimension of the islands. Figure 3(d) shows that indeed a power law fits our results quite well. However, the fractal dimension that the value of the exponent implies ($d_f = 0.8$) is unphysical. This means that the analysis of Tang is not suited for our model where islands diffuse. Instead, Villain *et al.*[6] have calculated the value of the exponent when dimers are allowed to diffuse. They find $\zeta = 2/5$, which is very close to our value of $\zeta = 0.42$. It is interesting to note that the importance of cluster diffusion had already been pointed out by Stoyanov *et al.*[1] long ago. They noticed that: "At present, there is considerable experimental evidence that, under favorable conditions, dimers, trimers, and even clusters with diameters up to 50–100 Å can migrate on the substrate as entities. This random motion of the clusters may be an important factor in the overall kinetics of thin film growth (...). For instance, in Sec. 6 we saw that, owing to cluster migration, at higher temperatures the saturation cluster density can be lower than expected from growth coalescence of immobile clusters." This is precisely the effect that we observe in the present model.

Coverage at maximum island density. There is another difference with the case where only monomers are allowed to move. Tang points out that the maximum density of islands should take place for a roughly constant value of the coverage, since the number of islands starts to decrease only when they start to coalesce. This can only be achieved, in systems where cluster mobility is absent, when islands occupy a significant fraction of the total area, i.e., at constant coverage (Tang takes the value 0.25). We have checked that this is actually a reasonable assumption. Cluster diffusion modifies the situation dramatically as is shown in Fig. 4. Here, the maximum number of islands is obtained for coverages that change by more than a factor of 100! This is understandable since now cluster diffusion allows island coalescence even at the first stages of growth. We stress that this dramatic modification of the dynamical evolution of island density only requires *small* cluster mobility, since for the coverages where the island density reaches its maximum, the mean cluster size is around 10. This can be checked from Fig. 4 by noting that, by definition of the mean island size S, one has the relationship $S = (\theta - N_{\text{mono}})/N_{\text{isl}}$ which implies $S < \theta/N_{\text{isl}}$. Then, this particular island evolution should be observed in many experimental systems, since it only requires that small clusters can move.

Mean cluster size. Another discrepancy with the rate equation analysis is the following: it is expected that the mean island size increases roughly as a power law of the coverage. Bartelt and co-workers[4] actually find an exponent close to 2/3. We have checked that this is indeed the case when only monomers diffuse ($\gamma = \infty$). Instead, in the DDA model, for $\gamma = 1$, we find that the mean size of the cluster distribution increases *exponentially* with

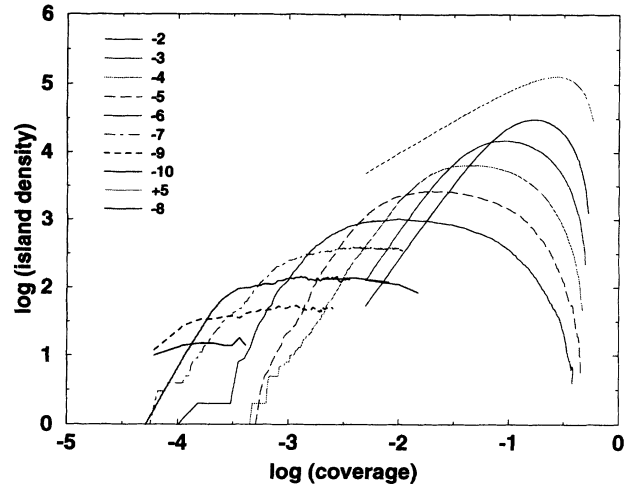

FIG. 4. Island density as a function of the coverage for several values of the normalized flux ($\gamma = 1$). The value of the coverage for which the island density reaches its maximum changes dramatically with the flux, passing from 0.3 for $\phi = 10^{+5}$ to 0.0001 for $\phi = 10^{-10}$.

coverage (Fig. 5). A possible explanation is that here the mean island size not only increases by single particle addition, which would be consistent with a power law, but also by *cluster* coalescence, even at the early stages of the growth. Then one could argue that the increase of the island mean size is proportional to the actual size of the island, generating an exponential increase. This exponential increase is very peculiar since usually, in growth models[17] power laws are found, for example in the CCA model.

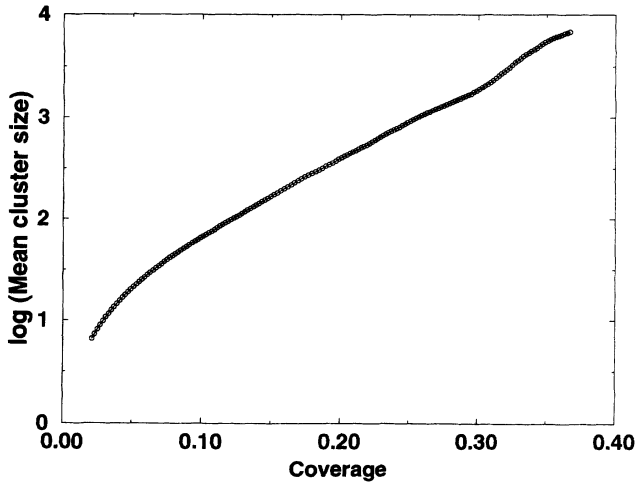

FIG. 5. Mean cluster size as a function of time for a normalized flux $\phi = 10^{-5}$, and a system size $L = 1000$ ($\gamma = 1$). The mean size is defined as $\langle s \rangle = \sum s N_s / N_s$ where N_s is the number of clusters containing s particles. It can be seen that, for coverages larger than roughly 5%, the cluster mean size increases *exponentially* with time.

Experimental tests of cluster mobility. We have seen in the previous paragraphs that the introduction of cluster diffusion leads to dramatic effects that were not previously studied and could be investigated experimentally. It is interesting to note that these dramatic effects are expected even if only small clusters can diffuse. Specifically, we think of three different possibilities: (i) Measuring the mean cluster size as a function of the coverage. A power law dependence would be compatible with exclusive monomer diffusion, whereas an exponential dependence would reveal that large clusters can diffuse. (ii) Similarly, it would be also interesting to study the dependence of the maximum island density on the deposition parameters (flux, temperature) and to compare them with the different models. (iii) An even more interesting test would be to study the island density as a function of coverage for low normalized fluxes (typically less than 10^{-5}): if the maximum is reached only at roughly a coverage of 0.2, this indicates that only monomers can move. On the contrary, if this maximum is reached for *smaller* values of the coverage and if this coverage becomes smaller as the flux decreases, then we guess that cluster diffusion has to be taken into account. We believe that this last test is realistic since the precise morphology of the clusters (compact or fractal) is not relevant here since we only deal with small clusters.

To summarize this section, we have found that at short times "nucleation centers" separated by a typical distance grow on the substrate. Then, blobs grow on these nucleation centers and the fractal dimension of these blobs increases monotonically from 1.5 to 1.9 as time increases until the percolation threshold. We have demonstrated that other dynamical analysis than that of the rate equations are needed to account for these results and we have proposed experimental tests that can show whether cluster diffusion is relevant to each specific experimental system.

IV. PROPERTIES AT SPANNING

It is clear that the properties of the system at the spanning point are the result of the growth processes studied in the preceding section. The focus on the percolation threshold is important both from experimental and theoretical points of view. Experimentally, the percolation threshold is a fundamental quantity for investigating the growth mechanisms of thin films prepared by deposition. As an example, Hashimoto and Hohara[26] used the percolation threshold—as measured by conductance measurements—to systematically study the influence of the experimental conditions on the growth properties of antimony thin films. The percolation threshold also indicates the metal-insulator transition at which metallic thin films show an anomalous optical behavior.[27] For a more comprehensive discussion, see the review by Smilauer.[28] Thus, experimentally, it seems very important to focus on the properties of the system at the percolation threshold. From the theoretical point of view, it is interesting to find out how diffusion affects the widely used percolation model, in which particles are deposited

on a surface but are not allowed to move. Our study shows that cluster diffusion significantly changes the percolation picture at criticality by introducing *two* typical length scales.

We find that, for a fixed flux, the morphology of the system at the spanning point changes as a function of the system size. We define the spanning time (or spanning "point") as the first time at which a cluster spans the whole lattice, i.e., contains sites on every column (we use periodic boundary conditions). Figure 6 shows the dependence of the total coverage θ_T and the spanning cluster coverage $\theta_{\rm PC}$ as functions of the system size *at the spanning time.* (We define the spanning cluster coverage as the number of sites of the spanning cluster divided by L^2.) We find three characteristic regimes, delimited by two crossover length scales L_1 and L_2: we will see later that L_1 is related to the characteristic diffusion length of a single particle on the surface, while L_2 emerges from the competition between deposition and *cluster* diffusion. The dependence of these two length scales with the normalized flux is studied in Sec. IV D.

Much of the knowledge about the behavior of the model at the spanning point can be summarized by the following picture [Fig. 7(a)]. We find that the system at the spanning time is equivalent to a *bond* percolation network of blobs, where the blobs are clusters of a typical length L_1 and a fractal dimension that depends on the system size. This can be seen in Fig. 7(b) where the ratio $\theta_{\rm PC}$ / θ_T is plotted for many different fluxes as a function of the effective system size L/L_1. All the different curves obtained for the different fluxes fall into a *single*, universal curve when rescaled by the "natural" length unit L_1. We argue that, for all the different fluxes, the systems at the spanning threshold are made up by blobs of a linear dimension L_1 that depends on the flux but with the same fractal dimension. The fractal dimension of the blobs does depend on the system size. The total coverage is given by

$$\theta_T(L) = \frac{1}{L^2} n_T^{\rm bl}(L, L_1) m^{\rm bl} = \frac{\alpha}{L_1^2} M_0 L_1^{D_f(L)} , \qquad (3)$$

where $m^{\rm bl}$ is the mass (number of sites) of a blob and $n_T^{\rm bl}$ is the *total* number of blobs present in the system, which is proportional to the size of the system ($n_T^{\rm bl} = \alpha L^2$). By definition of the fractal dimension, $m^{\rm bl} = M_0 L_1^{D_f(L)}$, where M_0 is a constant. Similarly, the coverage of the percolating cluster is given by

$$\theta_{\rm PC}(L) = \frac{1}{L^2} n_{\rm PC}^{\rm bl}(L, L_1) m^{\rm bl} = \beta \frac{\alpha}{L_1^2} M_0 L_1^{D_f(L)} , \qquad (4)$$

where $n_{\rm PC}^{\rm bl}$ is the number of blobs connected to the spanning cluster and β is the *ratio* of blobs that are connected to the percolating cluster to the total number of blobs. Figure 7(b) demonstrates that β is independent of the system size properly scaled by L_1, i.e., that the systems generated for different fluxes are similar in this sense. Next we study how the system size affects the precise morphology of the blobs, i.e., affects their number and their fractal dimension.

A. Regime I: "Particle diffusion regime" ($L < L_1$)

In this regime, only one cluster is present in the system. This fact is seen in Figs. 8 (a) and (b) and is also supported by Fig. 6: the total and spanning cluster coverages are superposed. Since the characteristic diffusion length of a single particle L_1 is larger than the system size L, every deposited particle attaches to the already existing cluster before the next particle is deposited. At short times, the cluster is small, and virtually all the particles are deposited outside the cluster and reach it by Brownian diffusion, so we expect that the cluster should have features in common with DLA. Indeed, at short times, we find that the cluster resembles DLA [Fig. 8(a)]. Its fractal dimension, measured by the sandbox method[17] is found to be 1.7, in agreement with the expected value for a DLA cluster.[17] At longer times, when the size of the cluster becomes comparable to the system size, a larger fraction of particles are deposited *inside* the cluster. Therefore, the model cannot be precisely the same as DLA, e.g., at the

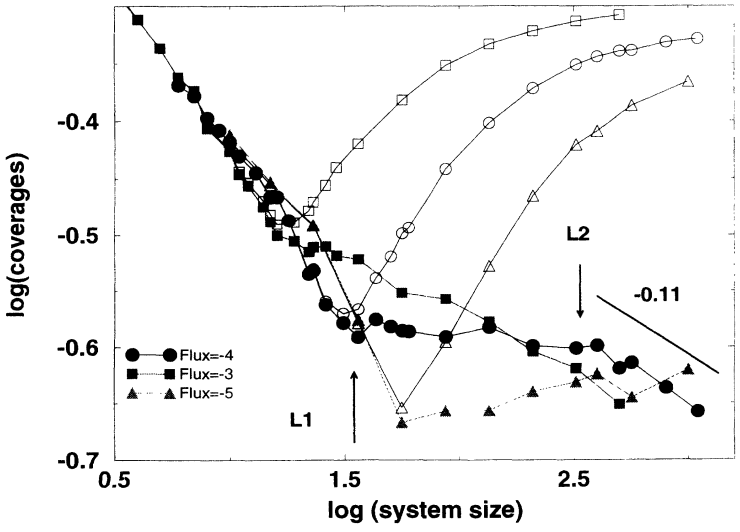

FIG. 6. Total coverage (open symbols) and coverage of the spanning cluster (full symbols) at the spanning time as a function of the system size L for three different values of the normalized flux ϕ: $10^{-3}, 10^{-4}$, and 10^{-5}. The arrows indicate the values of the two length scales L_1 and L_2 for $\phi = 10^{-4}$. The line on the right indicates the slope -0.11 that would be expected in the percolation model for the density of the spanning cluster as a function of L.

time of spanning, almost all new particles are deposited inside the boundaries of the cluster [cf. Fig. 8(b)].

B. Regime II: "Cluster diffusion regime" ($L_1 < L < L_2$)

Now several clusters are present in the system, as can be seen in Figs. 8(c) and (d). This can also be inferred from Fig. 6: at L_1 the curves for the different coverages split, indicating that, in addition to the spanning cluster, there are other clusters contributing to the total coverage. The reason for this is that the diffusion length is now smaller than the system size, so that several clusters nucleate on the surface. The spanning cluster is mainly built by the accretion of the diffusing blobs [Fig. 8(d)]. Moreover, we find that the fractal dimension of the blobs increases as the system size increases [Fig. 9].

C. Regime III: "Percolation regime" ($L > L_2$)

At short times, many clusters are present in the system [Fig. 8(e)], and, as the system is bigger, their number is

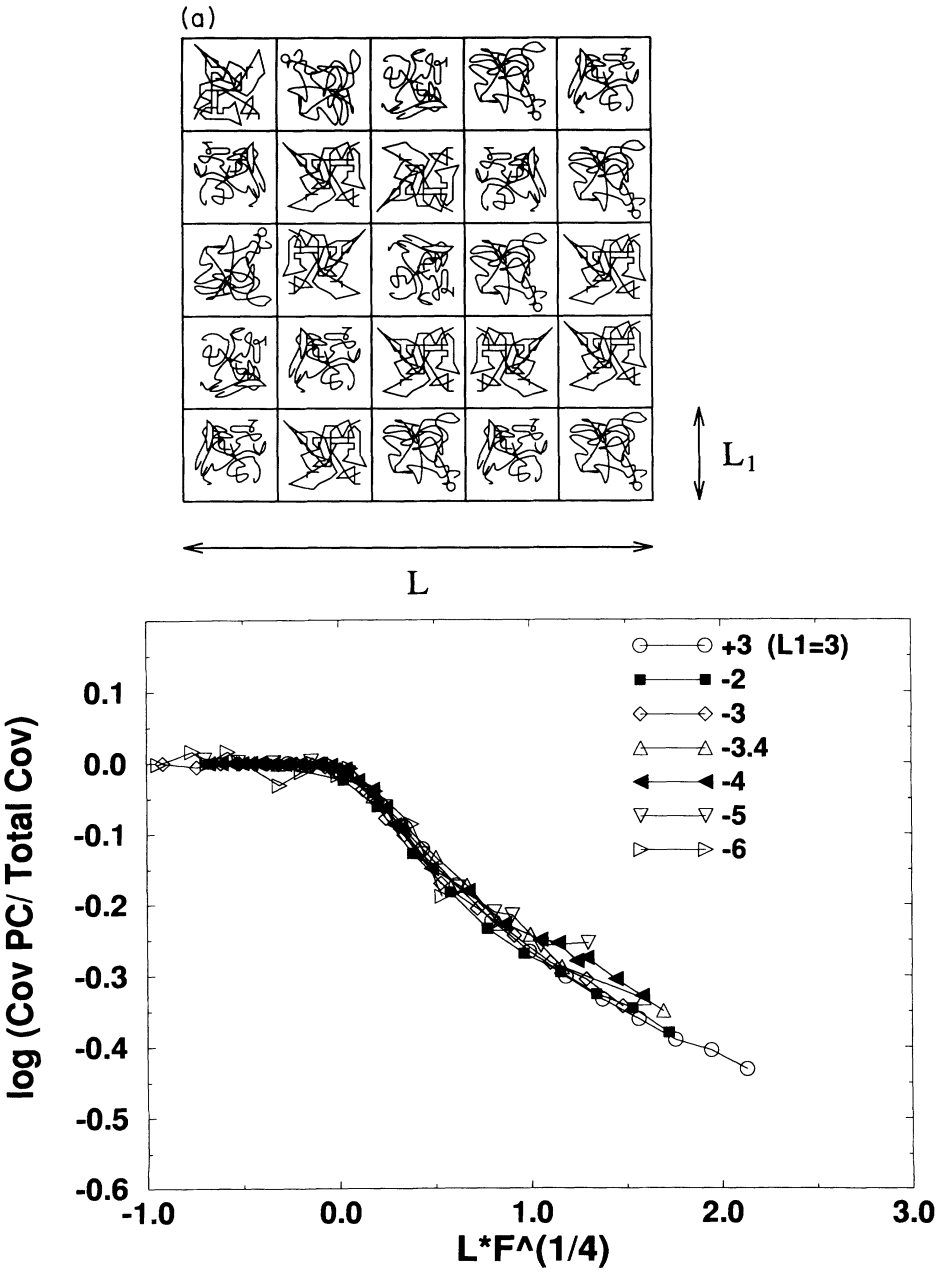

FIG. 7. (a) Schematical picture of the blob model for the system at the percolation threshold. (b) Ratio of the spanning cluster coverage to the total coverage versus the scaled system size. A value $L_1 = 3$ has been taken for the curve $F = 10^{+3}$. We use here the scaling relation $L_1 \sim \phi^{-1/4}$ [Eq. (7)] which is investigated in Sec. III D.

higher than in regime II. As time increases, bigger clusters are formed both by the connection of clusters that diffuse and by the addition of single deposited particles. At the spanning time, the system resembles a percolation network [Fig. 8(f)]. This resemblance is supported by the fact that, in this regime only, we find behaviors characteristic of a percolation system. For example, the slope of the spanning cluster coverage as a function of the system size becomes close to -0.11 (Fig. 6) as predicted by percolation.[14] Moreover, we find that only in this regime, the mean square deviation δ

$$\delta \equiv [\langle p_c(L)^2 \rangle - \langle p_c(L) \rangle^2]^{1/2} \tag{5}$$

(where the average is taken over many different configurations) varies with the system size as $\delta \sim L^{-1/\nu}$ with $\nu \simeq 1.3$, [Fig. 10(a)] which is in good agreement with the

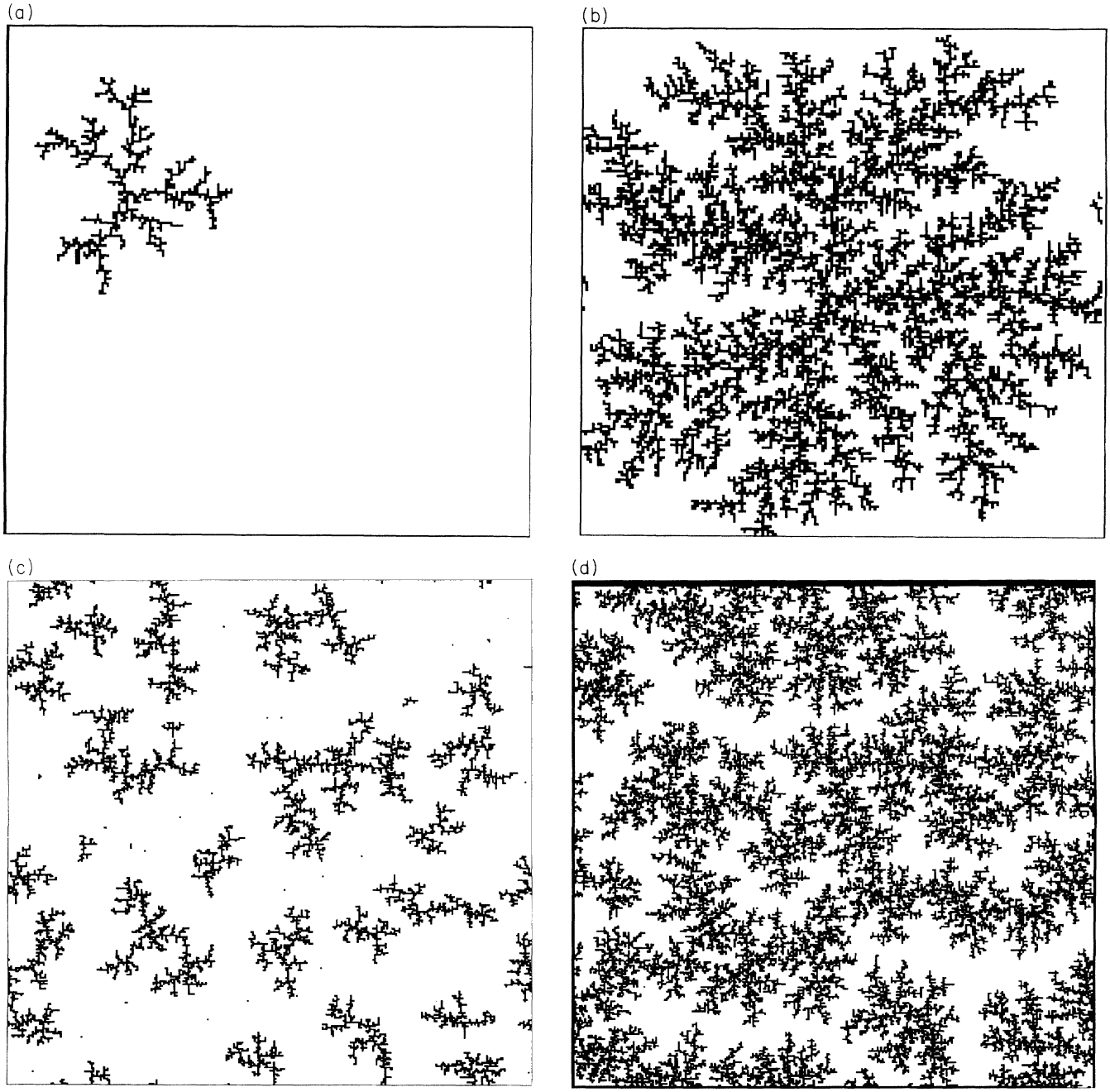

FIG. 8. System morphologies in the three regimes: (a) and (b) regime I; (c) and (d) regime II, (e) and (f), regime III. *Regime I (system size smaller than L_1)*: shown are two stages of the growth for $\phi = 10^{-9}$ ($L_1 \simeq 500$) and $L = 200$. (a) Total coverage=0.02, (b) spanning point: total coverage=0.27. *Regime II (system size between L_1 and L_2)*: shown are two stages of the growth for $\phi = 10^{-6}$ ($L_1 \simeq 90$ and $L_2 \simeq 10^4$) and $L = 300$. (c) Total coverage=0.1, (d) spanning point: total coverage=0.31. *Regime III (system size larger than L_2)*: shown are two stages of the growth for $\phi = 10^{-3}$ ($L_1 \simeq 17$ and $L_2 \simeq 36$) and $L = 300$. (e) Total coverage=0.1 (f) spanning point: total coverage=0.49. For all six figures, we choose $\gamma = 1$.

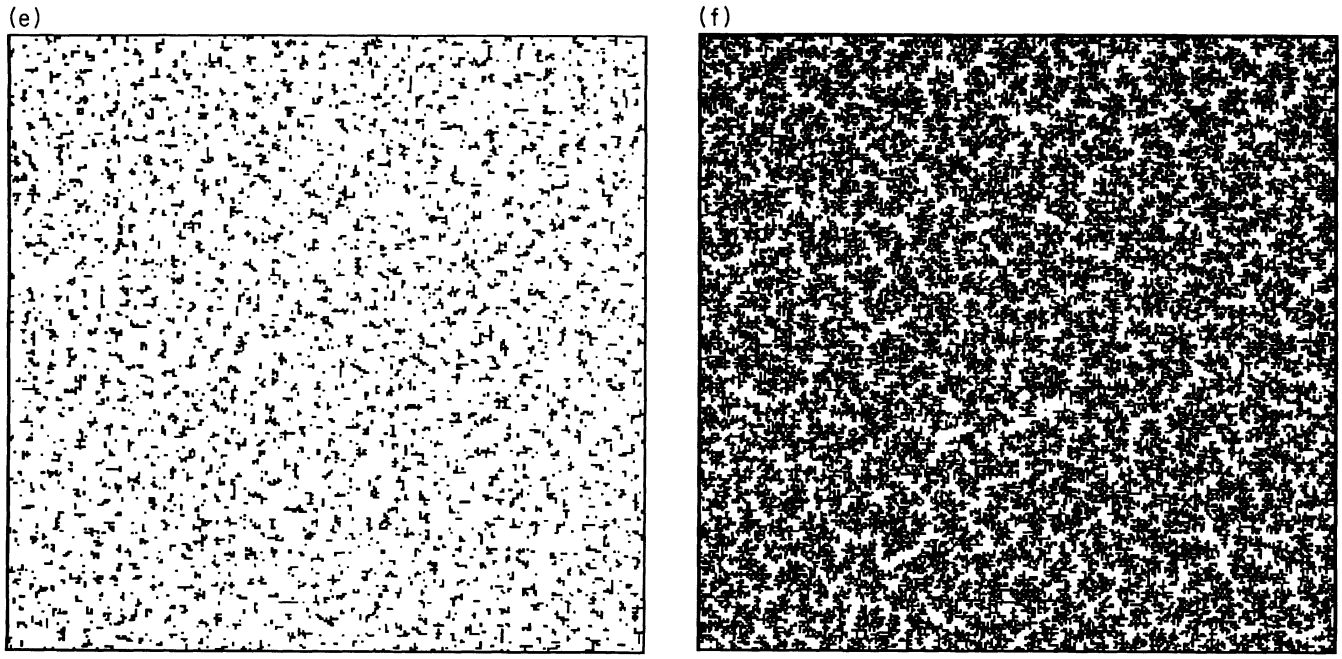

FIG. 8 *(Continued).*

exponent 4/3 predicted by percolation.[14] The total coverage also changes as predicted by the percolation model: *linearly* with δ for $L > L_2$: $p_c(L) - p_c(\infty) \sim \delta$ [Fig. 10(b)].[14] Thanks to this analogy with the percolation model, we can extrapolate the values of the coverage to infinite systems. According to the "blob picture" [Fig. 7(a), Eq. (3)], the total coverage at spanning for an infinite system should scale as

$$p_c(\infty) \sim L_1^{D_f-2} \sim F^{(2-D_f)/4}, \tag{6}$$

where we have used the scaling law [Eq. (7)] to be studied in Sec. IV D. From the simulations, we can estimate $p_c(\infty)$ as the intercept with the vertical axis for $\delta = 0$ in Fig. 10(b). Figure 11(a) shows that indeed the total coverage for an infinite system scales with the flux according to Eq. (6) and the slope of Fig. 11(a) gives $D_f(\infty) = 1.92$, in good agreement with the fractal dimension of percolation clusters ($D_f = 1.89$). The fractal dimension of the blobs can also be investigated directly using the sandbox method.[17,29] Figure 11(b) shows the density of the spanning cluster as a function of the box size l for several fluxes. It can be noticed that the plots indicate the existence of two regimes: for $3 \leq l \leq L'$, the curve is a straight line, while for $l \geq L'$, the density is first roughly constant and then decreases rapidly. The explanation is as follows: for $l \leq L'$, we see the structure of the blobs.

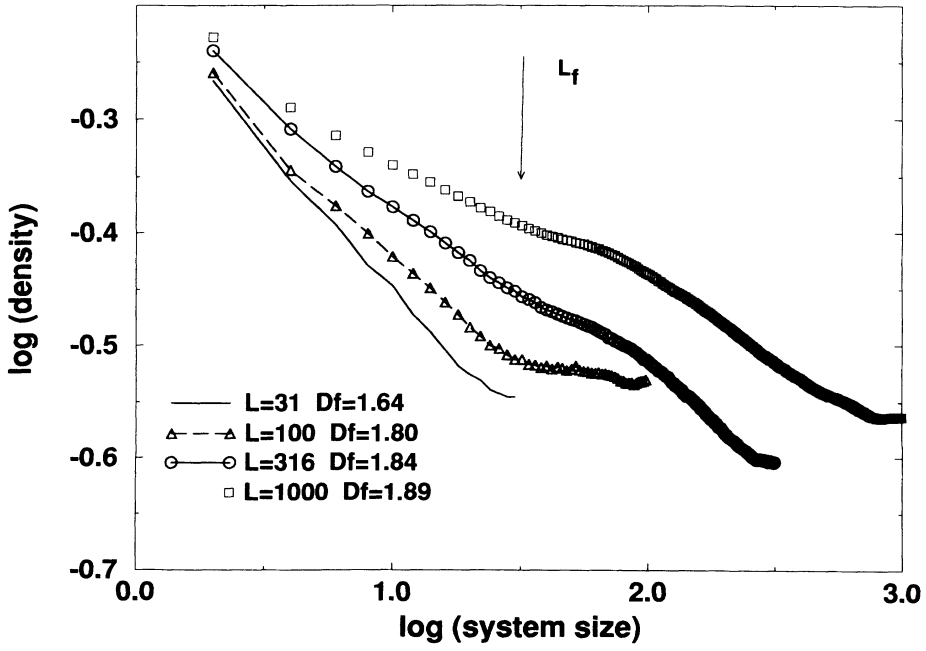

FIG. 9. Fractal dimension of the spanning cluster obtained by the sandbox method (Ref. 17) for four different system sizes and a normalized flux $\phi = 10^{-5}$. The spanning cluster is fractal up to a length scale L_f which remains approximately constant when L changes, but its fractal dimension continuously increases as L increases.

For larger l we should see the structure of the spanning cluster. However the latter is hidden by finite-size effects. From the small l behavior, we infer that the fractal dimension of the blobs for a very large system ($L = 1000$) is about 1.9 ± 0.03 which is in very good agreement with the value found from Fig. 11(a). Thus, we find from these two measurements that the fractal dimension of the blobs in the percolation regime is similar to the fractal dimension of percolation clusters ($D_f = 1.89$). The reasons for this agreement are not clear. From Figure 11(b) we also check that the linear dimension of the blobs (L') increases as F decreases. Actually, we find that L' is equal to the L_1 defined previously.

D. Phase diagram

Figure 6 shows results obtained for fluxes $\phi = 10^{-3}$, 10^{-4}, and 10^{-5}, but similar results have been obtained for the other fluxes we have studied ($10^{-6} \leq \phi \leq 10^{+5}$). We find that a change of the flux affects the values of the two crossover lengths L_1 and L_2. We have determined L_1 and L_2 for several fluxes: the results are presented in Fig. 12. The dependence of L_1 on ϕ can be understood by noting that the time needed by a single deposited particle randomly diffusing to explore the whole system is proportional to the system area and inversely proportional to the diffusion coefficient, $t_{\text{diff}} \simeq L^2/D_1$. By definition of the flux, the average time at which another particle is added to the system is $t_{\text{dep}} = 1/(FL^2)$. If $t_{\text{diff}} \ll t_{\text{dep}}$, the particle has sufficient time to explore the whole system (and, therefore, find an already existing cluster) before another particle is added. Consequently, a single cluster is built. If $t_{\text{diff}} \gg t_{\text{dep}}$, the particle finds another deposited particle before having had time to explore the whole system. Then several clusters are formed: this corresponds to regime II. The crossover between the two regimes occurs when these two times become comparable. This occurs for

$$L_1 \sim \phi^{-\psi_1}, \tag{7}$$

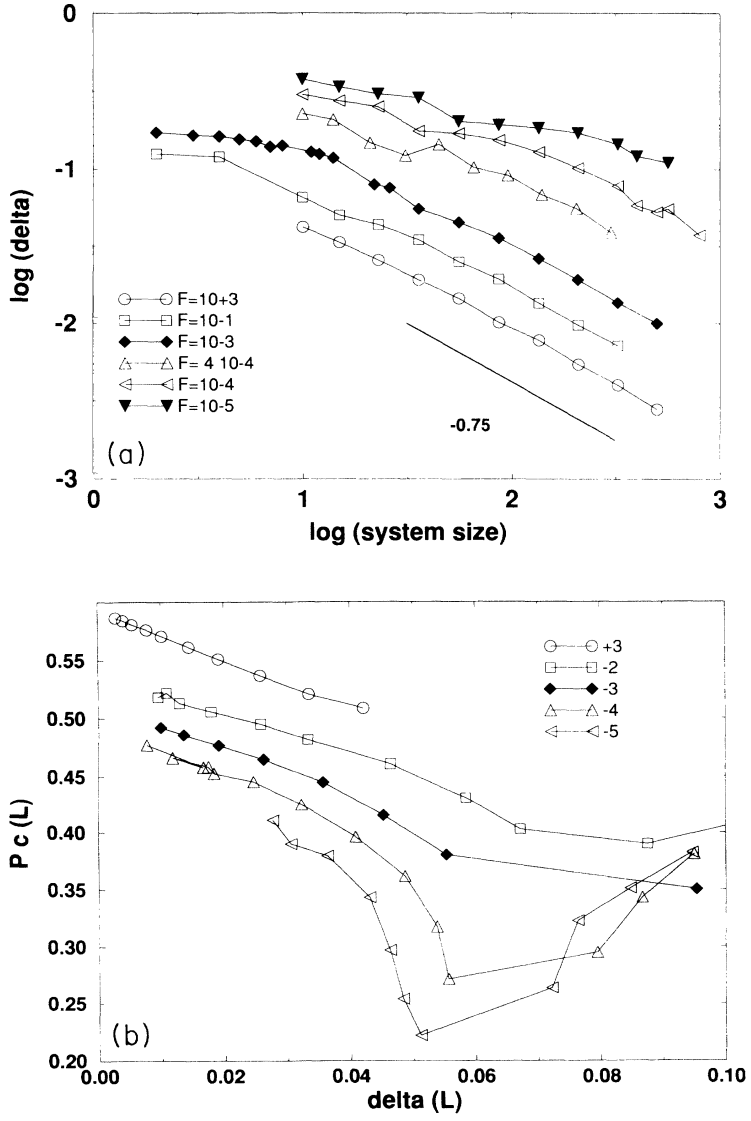

FIG. 10. (a) Log-log plot of δ (mean square deviation of the total coverage at spanning) vs the system size. A linear relation is expected for percolation (Ref. 14). This linear relation is observed only for systems larger than L_2. The solid line shows the slope expected from the percolation theory: $1/\nu = 3/4$. (b) Variation of the total spanning coverage as a function of its mean square deviation for different system sizes. A linear dependence, characteristic of percolation, is only found for $L > L_2$. The intercept of the straight part of the plot with $\delta = 0$ gives the spanning threshold for an infinite system (Ref. 14).

where $\psi_1 = 1/4$ in excellent agreement with the numerically obtained exponent of 0.24 ± 0.02 (Fig. 12). L_1 can be interpreted as the length scale determined by the competition between particle deposition (t_{dep}) and *single* particle diffusion (t_{diff}).

The second length scale L_2 also scales with the flux,

$$L_2 \sim \phi^{-\psi_2}, \tag{8}$$

where $\psi_2 = 0.9 \pm 0.2$ for $\gamma = 1$. We find that ψ_2 decreases as γ increases, unlike ψ_1 which is independent of γ. To uncover a physical interpretation of L_2, we fix the flux and change the system size. For spanning to occur, we must grow a cluster of size comparable to the system size. If the system is large, the clusters become large and, therefore, their diffusion coefficient becomes extremely small. In this limit, deposition dominates and connects the system in a percolationlike way. For smaller systems, the clusters are also smaller; they can move and connect one another to build clusters of sizes comparable to that of the system. Then diffusion dominates the connectivity of the system. The boundary between these two system sizes is set by L_2. Then, L_2 can be interpreted as the length scale determined by the competition between particle deposition and *cluster* diffusion. This analysis is supported by the fact that the second crossover L_2 is not observed when only single particles are allowed to move, thereby suppressing the possibility that the connections are made by cluster diffusion.

Based on the previous results, we may now construct a "morphology phase diagram" that serves to characterize the morphology of the system at the spanning time in terms of the two tuning parameters L and ϕ (Fig. 12). The three regimes, I–III, are delineated by the two crossover lines, $L_1(\phi)$ and $L_2(\phi)$, which intersect at a "critical point" whose coordinates, (ϕ_c, L_c), depend only on γ. Thus for a fixed system size L, two situations can arise, depending on the value of γ. (i) If $L \ll L_c(\gamma)$, then the system shows a direct transition from the single cluster regime to percolation as the normalized flux ϕ increases. (ii) If $L \gg L_c(\gamma)$, then regime II can also be observed for intermediate values of the normalized flux.

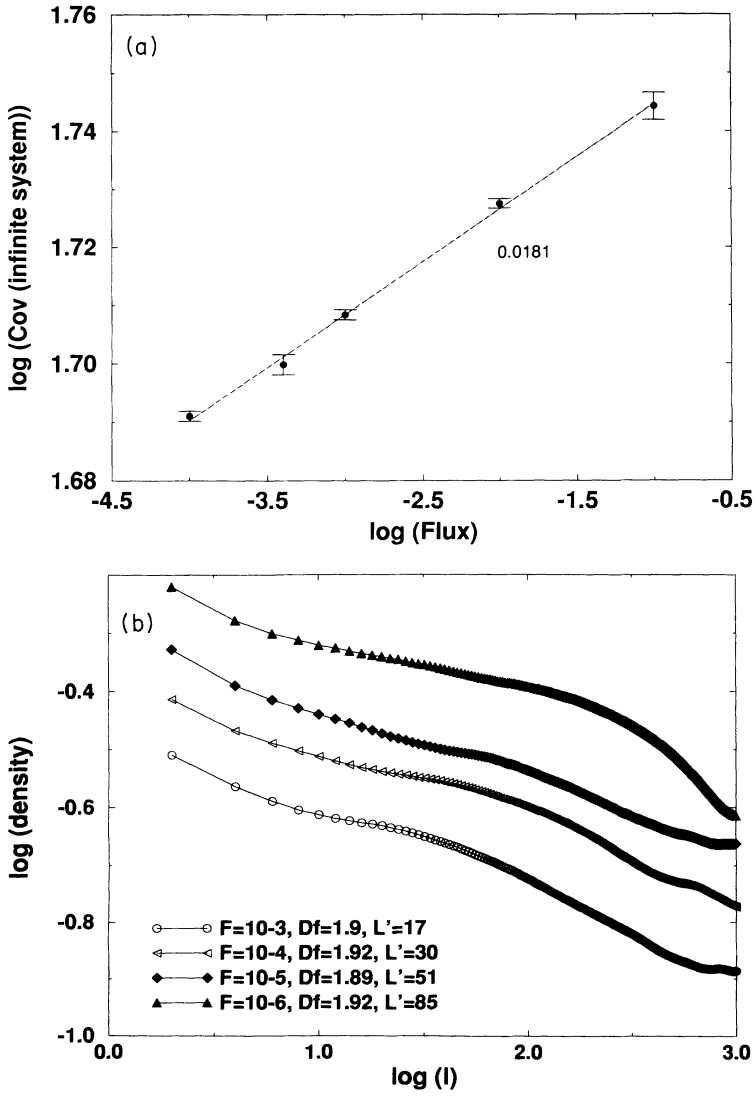

FIG. 11. (a) Spanning threshold for an infinite system versus the normalized flux. From the slope of the best fit and Eq. (6), we deduce the fractal dimension of the blobs for an infinite system: 1.92. (b) Sandbox (Ref. 17) density plots of the spanning clusters obtained for a system size $L = 1000$ and several fluxes. The curves are shifted for a better visualization. L' is obtained as the maximum of the derivative of $c(l)$, i.e., the value of the derivative that is closer to 0. This would correspond to a constant value of $c(l)$ which would be ideally obtained if no finite-size effects were present.

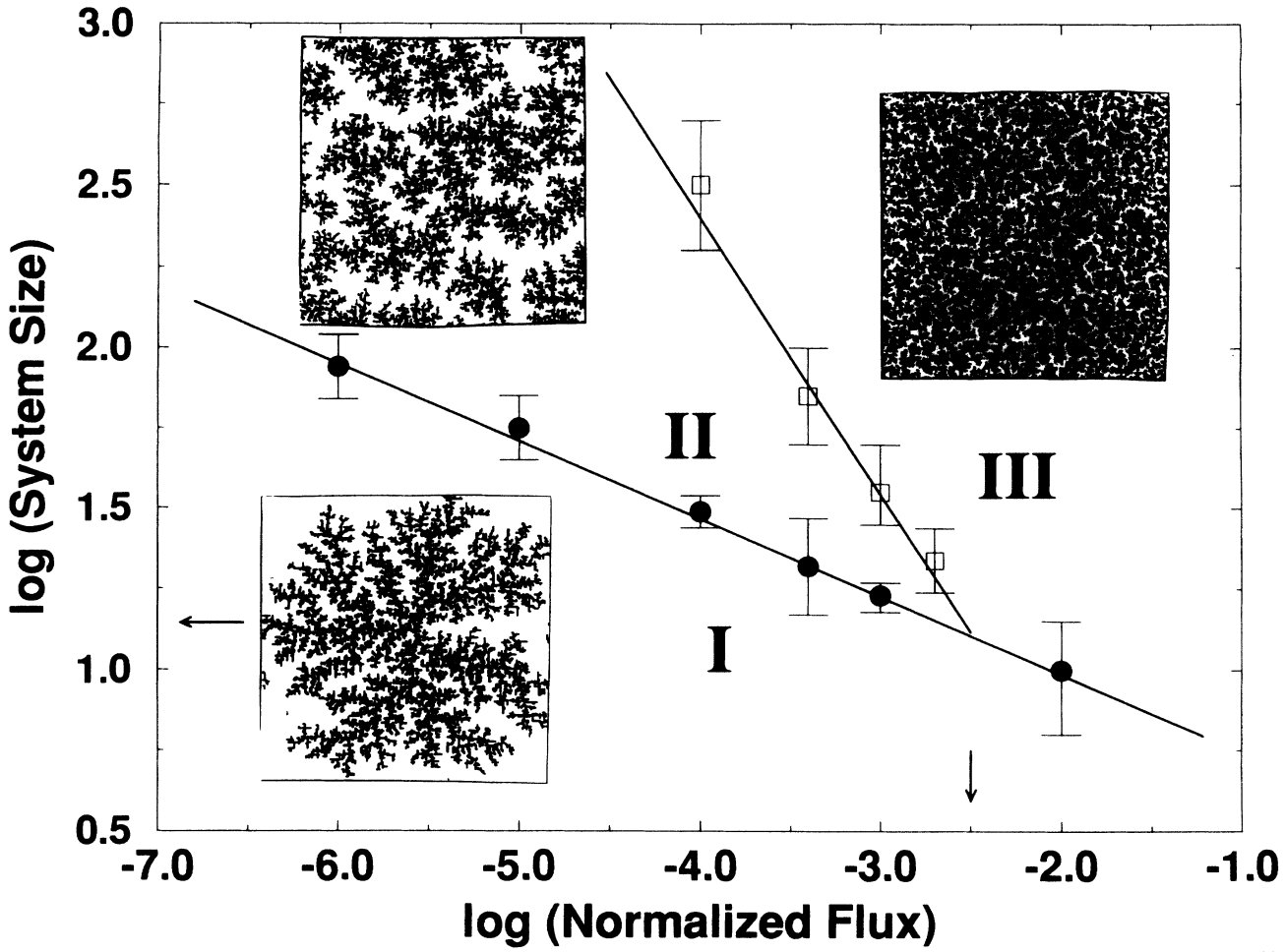

FIG. 12. The (ϕ, L) phase diagram for $\gamma = 1$. Shown is the dependence on normalized flux of the two length scales L_1 (full circles) and L_2 (open squares). The lines separating the three regimes I–III have been obtained by linear fits of the data for L_1 (slope $\psi_1 = 0.24 \pm 0.02$) and L_2 (slope $\psi_2 = 0.9 \pm 0.2$). The arrows indicate the critical values ϕ_c and L_c. The insets show typical morphologies for each regime.

V. DISCUSSION AND CONCLUSION

In summary, we have proposed a model that describes the diffusion-controlled aggregation exhibited by particles as they are deposited on a surface. The model, which incorporates deposition, particle and cluster diffusion, and aggregation, is inspired by recent thin-film-deposition experiments that use a low-energy cluster beam deposition (LECBD) technique.[12] We find that the model permits one to distinguish the effects of deposition, diffusion and aggregation, and that tuning the relative strength of, e.g., deposition and diffusion, generates a rich range of morphologies—including diffusion limited aggregation, cluster-cluster aggregation, and percolation. The length and time scales characterizing these morphologies depend on such experimentally controllable parameters as deposition flux and diffusion constant, raising the possibility that the model may prove useful in future studies seeking the controlled design of nanostructure morphologies. We can argue that the DDA model is suited for (i) MBE by taking large γ values, (ii) other deposition experiments where edge diffusion is absent: the structures obtained in Figs. 8(c) and (e) (low coverages) resemble some experimental images obtained by LECBD (see Fig. 3 of Ref. 21, and Fig. 1 of Ref. 22) on substrates held at low temperatures, (iii) all the dynamic properties related to *small* cluster diffusion on surfaces such as those presented in Sec. III. (iv) Rigid large-cluster diffusion is not realistic for clusters on surfaces: the investigation of its effects (Sec. IV) at the spanning point, resulting in the new phase diagram may be interesting for other experimental systems such as colloids.

Note added in proof. After this work was submitted, Bales and Chrzan[30] published a clear study of modified rate equations.

ACKNOWLEDGMENTS

We wish to thank C. Henry, J. Kertész, D. Stauffer, and A. Vespignani for helpful discussions. P.J. acknowledges CNRS and NATO for financial support. H.L. thanks CONACYT, Mexico, for support. A.-L.B. and H.E.S. thank the Hungary-U.S.A. exchange program of the Hungarian Academy of Sciences. S.H. acknowledges the U.S.A.-Israel Binational Science Foundation for financial support. The Center for Polymer Studies is supported by NSF.

* Permanent address: Département de Physique des Matériaux, Université Claude Bernard Lyon-1, Villeurbanne Cedex, France.
† Present address: IBM Thomas J. Watson Research Center, Yorktown Heights, NY 10598.
‡ Present address: Physics Department, Cavendish Laboratory, Cambridge University, Madingley Road, Cambridge CB3 0HE, England.
§ Permanent address: Physics Department, Bar Ilan University, Ramat Gan, Israel.

[1] S. Stoyanov and D. Kaschiev, in *Current Topics in Materials Science*, edited by E. Kaldis (North-Holland, Amsterdam, 1981).
[2] J. A. Venables, G. D. T. Spiller, and M. Hanbücken, Rep. Prog. Phys. **47**, 399 (1984); A.-L. Barabási and H. E. Stanley, *Fractal Approach to Surface Growth* (Cambridge University Press, Cambridge, in press).
[3] L.-H. Tang, J. Phys. I France **3**, 935 (1993). Tang's model has been studied extensively by J. G. Amar, F. Family, and P.-M. Lam, Phys. Rev. B **50**, 8781 (1994), and has been generalized to the case in which the clusters diffuse [P. Jensen, A.-L. Barabási, H. Larralde, S. Havlin, and H. E. Stanley, Physica A **207**, 219 (1994)].
[4] M.C. Bartelt and J. W. Evans, Phys. Rev. B **46**, 12 675 (1992); Surf. Sci. **298**, 421 (1993); M.C. Bartelt, M.C. Tringides, and J. W. Evans, Phys. Rev. B **47**, 13 891 (1993).
[5] J. Villain, A. Pimpinelli, and D. E. Wolf, Phys. Rev. Lett. **69**, 985 (1992).
[6] J. Villain, A. Pimpinelli, L.-H. Tang, and D. E. Wolf, J. Phys. I France **2**, 2107 (1992).
[7] S. V. Ghaisas and S. Das Sarma, Phys. Rev. B **46**, 7308 (1992).
[8] Y. W. Mo, J. Kleiner, M.B. Webb, and M.G. Lagally, Phys. Rev. Lett. **66**, 1998 (1991).
[9] *Kinetics of Ordering and Growth at Surfaces*, edited by M. Lagally (Plenum, New York, 1990); M. Lagally, Phys. Today **46** (11), 24 (1993); S. Das Sarma, J. Vac. Sci. Technol. A **8**, 2714 (1990).
[10] R. Q. Hwang, J. Schröder, C. Günther, and R. J. Behn, Phys. Rev. Lett. **67**, 3279 (1991); T. Michely, M. Hohage, M. Bott, and G. Comsa, *ibid.* **70**, 3943 (1993).
[11] H. Röder, E. Hahn, H. Brune, J.-P. Bucher, and K. Kern, Nature **366**, 141 (1993); H. Brune, C. Romainczyk, H. Röder, and K. Kern, *ibid.* **369**, 469 (1994); P. Jensen, A.-L. Barabási, H. Larralde, S. Havlin, and H. E. Stanley, *ibid.* **368**, 22 (1994); Phys. Rev. E **50**, 618 (1994).
[12] P. Melinon, P. Jensen, J. X. Hu, A. Hoareau, B. Cabaud, M. Treilleux, and D. Guillot, Phys. Rev. B **44**, 12 562 (1991).
[13] P. Meakin, Phys. Rev. Lett. **51**, 1119 (1983); M. Kolb, R. Botet, and R. Jullien, *ibid.* **51**, 1123 (1983); for a comprehensive review, see H. J. Herrmann, Phys. Rep. **136**, 153 (1986).
[14] D. Stauffer and A. Aharony, *Introduction to Percolation Theory* (Taylor and Francis, London, 1992).
[15] *Fractals and Disordered Systems*, edited by A. Bunde and S. Havlin (Springer-Verlag, Berlin, 1991).
[16] T. A. Witten and L. M. Sander, Phys. Rev. Lett. **47**, 1400 (1981).
[17] T. Vicsek, *Fractal Growth Phenomena*, 2nd ed. (World Scientific, Singapore, 1992).
[18] C. Chapon and C. R. Henry, Surf. Sci. **106**, 152 (1981); C. Reiners, Thin Solid Films **143**, 311 (1986).
[19] D. Kaschiev, Surf. Sci. **86**, 14 (1979).
[20] C. R. Henry, C. Chapon, and B. Mutaftschiev, Thin Solid Films **46**, 157 (1977).
[21] P. Jensen, P. Melinon, A. Hoareau, J. X. Hu, B. Cabaud, M. Treilleux, E. Bernstein, and D. Guillot, Physica A **185**, 104 (1992).
[22] L. Bardotti, P. Jensen, M. Treilleux, B. Cabaud, and A. Hoareau (unpublished).
[23] R. L. Schwoebel, J. Appl. Phys. **40**, 614 (1969); R. L. Scwoebel and E. J. Shipsey, *ibid.* **37**, 3682 (1966); J. Villain, J. Phys. I **1**, 19 (1991).
[24] M. C. Bartelt and J. W. Evans, Europhys. Lett. **21**, 99 (1993).
[25] It should be stressed that, contrary to the case where only monomers diffuse (Ref. 3), the definition of a "nucleation center" is not that sharp.
[26] H. Hashimoto and T. Hohara, Thin Solid Films **199**, 71 (1991).
[27] Y. Yagil, P. Gadenne, C. Jullien, and G. Deutscher, Phys. Rev. B **46**, 2503 (1992).
[28] P. Smilauer, Contemp. Phys. **32**, 89 (1991).
[29] A. Kapitulnik, A. Aharony, G. Deutscher, and D. Stauffer, J. Phys. A **16**, L269 (1984).
[30] G. S. Bales and D. C. Chrzan, Phys. Rev. B **50**, 6057 (1994).

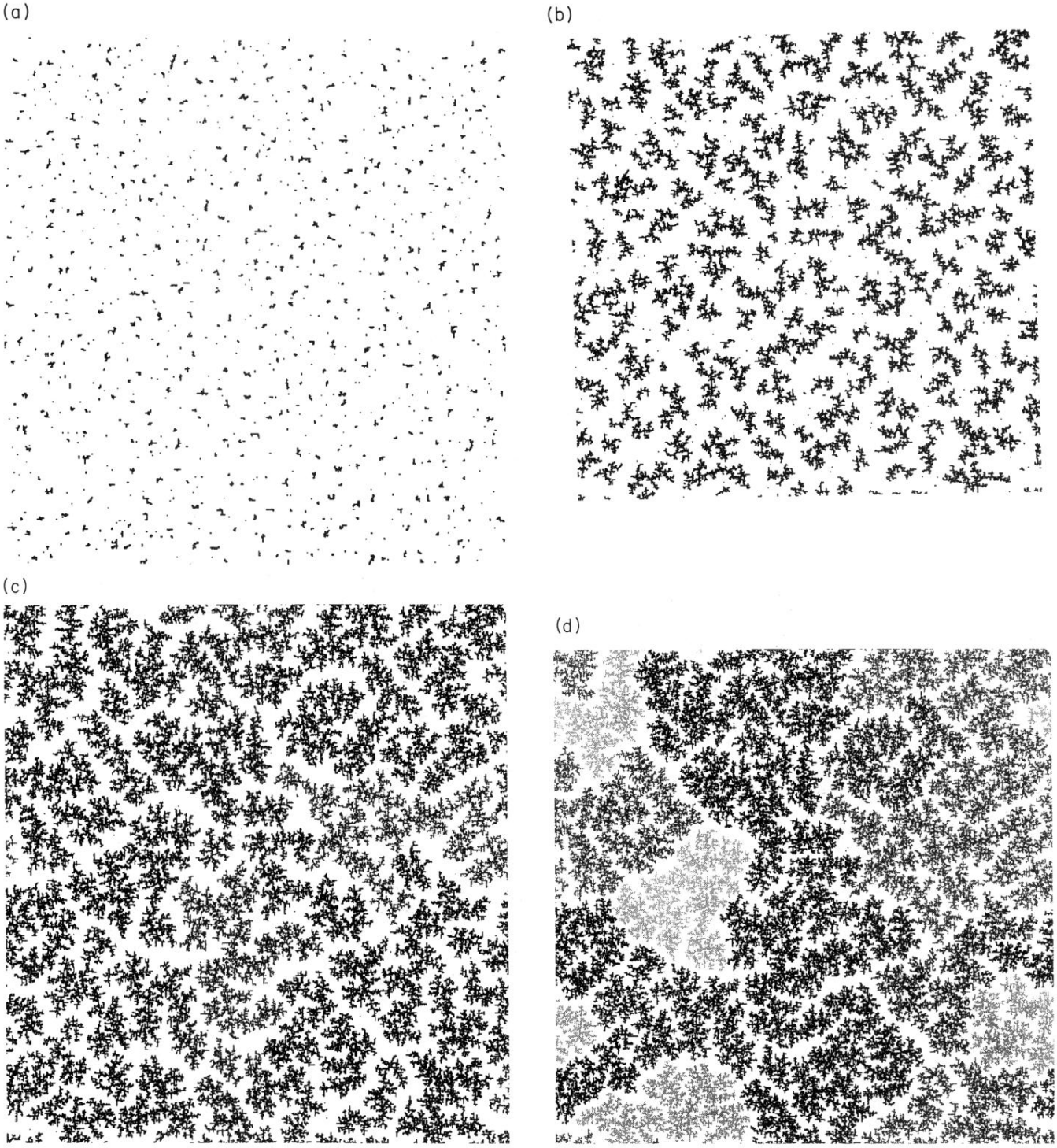

FIG. 2. Morphologies obtained for a normalized flux $\phi = 10^{-5}$, a system size $L = 500$ and $\gamma = 1$. Four different coverages (corresponding to four different times of deposition) are shown: (a) coverage 0.02, (b) coverage 0.15, (c) coverage 0.35, and (d) coverage 0.43 (spanning point).